EBioMedicine 48 (2019) 23–35

Contents lists available at ScienceDirect

EBioMedicine

journal homepage: www.elsevier.com/locate/ebiom

EBioMedicine
Published by THE LANCET

Research paper

Characterization of plasma-derived protoporphyrin-IX-positive extracellular vesicles following 5-ALA use in patients with malignant glioma

Pamela S. Jones[a,1], Anudeep Yekula[a,1], Elizabeth Lansbury[a], Julia L. Small[a], Caroline Ayinon[a], Scott Mordecai[b], Fred H. Hochberg[c], John Tigges[d], Bethany Delcuze[e], Alain Charest[e], Ionita Ghiran[e], Leonora Balaj[a,2,*], Bob S. Carter[a,2,*]

[a] Department of Neurosurgery, Massachusetts General Hospital, Harvard Medical School, Boston, MA, United States
[b] Department of Pathology, Flow Cytometry Core, Massachusetts General Hospital, Boston, MA, United States
[c] Scintillon Institute, La Jolla, CA, United States
[d] Flow Cytometry Core, Beth Israel Deaconess Medical Center, Boston, MA, United States
[e] Department of Medicine, Beth Israel Deaconess Medical Center, Harvard Medical School, Boston, MA, United States

ARTICLE INFO

Article history:
Received 30 May 2019
Revised 11 September 2019
Accepted 13 September 2019
Available online 15 October 2019

Keywords:
Extracellular vesicles
Malignant gliomas
Liquid biopsy
Imaging flow cytometry
5-ALA
Fluorescence guided surgery

ABSTRACT

Background: Malignant gliomas are rapidly progressive brain tumors with high mortality. Fluorescence guided surgery (FGS) with 5-aminolevulinic acid (5-ALA) provides fluorescent delineation of malignant tissue, which helps achieve maximum safe resection. 5-ALA-based fluorescence is due to preferential accumulation of the fluorophore protoporphyrin-IX (PpIX) in malignant glioma tissue. Additionally, gliomas cells release extracellular vesicles (EVs) which carry biomarkers of disease. Herein, we performed animal and human studies to investigate whether 5-ALA dosed glioma cells, *in vitro* and *in vivo*, release PpIX positive EVs in circulation which can be captured and analyzed.
Methods: We used imaging flow cytometry (IFC) to characterize PpIX-positive EVs released from 5-ALA-dosed glioma cells, glioma-bearing xenograft models, as well as patients with malignant glioma undergoing FGS.
Findings: We first show that glioma cells dosed with 5-ALA release 247-fold higher PpIX positive EVs compared to mock dosed glioma cells. Second, we demonstrate that the plasma of glioma-bearing mice ($n=2$) dosed with 5-ALA contain significantly higher levels of circulating PpIX-positive EVs than their pre-dosing background ($p=0.004$). Lastly, we also show that the plasma of patients with avidly fluorescent tumors ($n=4$) undergoing FGS contain circulating PpIX-positive EVs at levels significantly higher than their pre-dosing background ($p=0.00009$) and this rise in signal correlates with enhancing tumor volumes ($r^2=0.888$).
Interpretation: Our findings highlight the potential of plasma-derived PpIX-positive EV-based diagnostics for malignant gliomas, offering a novel liquid biopsy platform for confirming and monitoring tumor status.

Research in context

Evidence before this study

The US Food and Drug Administration (FDA) approved 5-aminolevulinic acid (5-ALA) as an intraoperative optical imaging agent in patients with suspected malignant gliomas. 5-ALA-based fluorescence guided surgery allows for improved resection of malignant gliomas by turning glioma tissue fluorescent pink under

Abbreviations: GBM, glioblastoma multiforme; 5-ALA, 5-aminolevulinic acid; PpIX, protoporphyrin IX, EV, extracellular vesicle; IFC, Image flow cytometry; HBMVEC, human brain microvascular endothelial cells; FGS, fluorescence guided surgery; ISX, Image Stream^x; sEVs, single EVs.

* Corresponding authors.
E-mail addresses: balaj.leonora@mgh.harvard.edu (L. Balaj), bcarter@mgh.harvard.edu (B.S. Carter).

[1] Co-first authors.
[2] These authors jointly supervised this work

https://doi.org/10.1016/j.ebiom.2019.09.025

blue light microscopy. Furthermore, it is well established that all cells release extracellular vesicles (EVs) both *in vitro* and *in vivo* and in the case of glioma cells, they carry biomarkers of disease burden. Characterizing tumor specific fluorescent EVs derived from the plasma of patients dosed with 5-ALA may provide a minimally invasive platform for the diagnosis of malignant gliomas.

Added value of this study

Herein we show that glioma cells, both *in vitro* and *in vivo*, exposed to 5-ALA secrete EVs that are also fluorescent. We first characterized 5-ALA dosed glioma cells and showed that fluorescent EVs are secreted from fluorescent glioma cells but not from normal cells. We also used xenograft models to show that fluorescent circulating EVs are present in the plasma of tumor bearing mice dosed with 5-ALA and were absent in control, non-tumor bearing mice. Finally, we collected plasma samples from patients undergoing fluorescent guided surgery for the resection of malignant gliomas at the Massachusetts General Hospital, pre and post 5-ALA administration. We show that, in the presence of an avidly fluorescing intraoperative tumor after 5-ALA administration, patients had a significantly higher number of fluorescent EVs in their plasma, and this fold increase highly correlated with their tumor volumes.

Implications of all the available evidence

We will continue to collect plasma samples from patients undergoing glioma resection using 5-ALA, both here at MGH as well as other institutions under our optimized plasma collection protocol which will reduce chances of bleaching the fluorescent signal. A larger cohort would validate the evidence for first-time glioma diagnosis as well as provide a framework for potential non-surgical delivery of 5-ALA to patients to monitor recurrence. Clinically, there is a major need for minimally invasive diagnosis of gliomas, and characterizing circulating tumor specific fluorescent EVs provides a window into the primary tumor.

1. Introduction

Malignant gliomas are highly aggressive central nervous system (CNS) neoplasms that rank among the deadliest human malignancies [1]. Surgery remains the first line of treatment for these tumors and can significantly extend patient survival if gross total resection of contrast-enhancing tumor is achieved [2]. The recent FDA approval of aminolevulinic acid hydrochloride, known as ALA HCl (Gleolan™; NX Development Corp.), provides the neurosurgeon with real-time fluorescent delineation of malignant tissue. Several studies indicate significantly higher rates of gross total resections of enhancing disease and longer progression-free survival for patients with malignant glioma who undergo FGS as compared to conventional white-light resections [3].

PpIX is a naturally-occurring fluorescent precursor in the heme synthesis pathway and accumulates in glioma tumor cells following administration of 5-ALA [4]. The underlying mechanisms behind the preferential accumulation of PpIX in glioma tissue but not normal tissue are multifactorial. It has been reported that a fragile blood brain barrier (BBB), common in malignant gliomas, combined with increased activity of GABA, pepT1, and pepT2 transporters greatly facilitate 5-ALA accumulation into glioma cells [5–7]. Furthermore, increased activity of ALA-dehydrogenase and porphobilinogen-deaminase, decreased activity of ferrochelatase and reduced availability of Fe^{2+} results in highly specific PpIX accumulation in glioma cells [8–14]. Recent studies have also highlighted the role of ABCG2 transporter in the shuttling of PpIX from the mitochondria into cytosol [6,15] and because of this tumor-specific uptake, there is a growing body of literature on the role of 5-ALA in diagnosis and treatment of many types of cancers [16–21]. With its fluorophore properties, PpIX yields a red-violet emission (λ=635 nm) following excitation with blue light (λ=400-410 nm). Thus, using a blue-light filter on an operative microscope, the neurosurgeon is able to distinguish tumor, which has excess PpIX and fluoresces pink, from normal brain, which does not have PpIX accumulation and, therefore, lacks fluorescence [22].

The recognition that EVs are present in a variety of biofluids has led to tremendous interest in exploiting them as a source of biomarkers for gliomas [23–31]. Ranging from 30 to 1000 nm in diameter, EVs are released into biofluids by organ-specific cell populations and contain genetic materials reflective of their cells of origin [32–34]. We hypothesized that EVs released from glioma cells following administration of 5-ALA contain PpIX, and this fluorescence could be a potential marker for glioma specific EV detection. The small size of EVs entails significant challenges for quantitative and qualitative analysis at the single vesicle level due to the detection limits of most instruments. Although flow cytometry offers opportunities for high-throughput analysis of single cells or particles, most conventional flow cytometers are not suited to detect the dim signals generated by small EVs [35]. Only recently has the capability of IFC been used to analyze single EVs (sEVs) [36–40]. We therefore sought to explore the advanced technology of IFC by using Amnis ImageStream MKII, which has the ability to analyze fluorescent nanoparticles, including EVs [36,41–43]. The advantage of this instrument lies in the detection of fluorescent signal from otherwise undetectable nanoparticle populations, allowing for sEV detection and multi-parametric phenotyping of sEV populations [41,44–46]. Through potential detection and precise quantification of EV subpopulations secreted by glioma cells, IFC may allow for a robust assay for the characterization of tumor specific EV subpopulations at the sEV level. The ability to study malignant gliomas on the sEV level is especially important given the significant intertumoral heterogeneity, both at a single time point as well as over the course of tumor treatment [47].

Our central hypothesis is: i) glioma cells cultured *in vitro* ii) plasma from glioma-bearing mice, and iii) plasma from patients harboring malignant gliomas can be evaluated for PpIX-positive EVs following administration of 5-ALA using IFC.

2. Materials and methods

2.1. Cell line

The human Gli36 glioma cell line (RRID:CVCL_RL88) was generated at Massachusetts General Hospital with approved IRB protocol and cultured in high glucose Dulbecco's modified essential medium (DMEM; Gibco, Invitrogen Cell culture, Carlsbad, CA) containing 10% fetal bovine serum (FBS; Life Technologies Corporation, Carlsbad, CA) and 1% Penicillin/Streptomycin (Penicillin Streptomycin Solution; Life Technologies Corporation, Carlsbad, CA). HBMVEC were kindly provided by Xandra O. Breakefield and cultured using endothelial basal medium (EGM-2 MV Microvascular Endothelial Cell Growth Medium-2 BulletKit, Lonza, Allendale, NJ). All *in vitro* experiments were performed with a cell confluency of 50–70% to minimize cell death. All the cell lines are periodically verified for mycoplasma contamination using commercial mycoplasma PCR (PCR Mycoplasma Detection Kit, Applied Biological Materials Incorporated, Richmond, British Columbia).

2.2. Dosing with 5-ALA

5-ALA (Sigma-Aldrich; Saint Louis, MO) was dissolved in 1 ml sterile filtered phosphate buffered saline (PBS 1x; Thermo Fisher

Scientific, Baltics UAB, Vilnius, Lithuania), aliquoted and stored at a concentration of 2.9 M at −20 °C. For dose determination experiments, Gli36 cells were plated in a 6-well plate (Corning Costar Flat Bottom Cell Culture plates; Corning Incorporated, Corning, NY) at a seeding density of 250,000 cells per well on day 0. Cells were allowed to grow for 24 h in the incubator at 37°C. On day 1, each well was washed with 1 ml PBS to remove floating cells and 1.8 ml of fresh DMEM/well was added. Cells were dosed with 200 μL of 5-ALA solutions from secondary stock concentrations to obtain final concentrations of 64 mM, 32 mM, 16 mM, 8.0 mM, and 0.8 mM in the first 5 wells. The last well was mock dosed with 200 μL filtered PBS. The final volume of each well was kept constant at 2.0 ml. Fluorescence intensity and viability were assessed 24 h after dosing. For the remaining experiments, Gli36 cells and HMBVEC were plated in P15 plates (Nunc Dish 150 mm, Thermo Fisher Scientific, Waltham, MA) at a seeding density of 5 million cells/plate. On day 1, each plate was washed with PBS, dosed with 0.8 mM concentration of 5-ALA or mock (filtered PBS) after replacing DMEM with 15% EV depleted Fetal Bovine Serum (FBS; Life Technologies Corporation, Carlsbad, CA). Conditioned media was collected 24 h after dosing. All experiments were performed in a dim light with the plates covered with aluminum foil at all times to avoid bleaching of PpIX fluorescence.

2.3. Cell viability

The cells were trypsinized (0.25% Trypsin-EDTA; Life Technologies Corporation, Carlsbad, CA) and the viability was assessed using Countess II FL Automated Cell Counter (Thermo Fisher Scientific, Waltham, MA).

2.4. Confocal microscopy

Cells were plated in glass bottom 6-well plate (VRW, Radnor Headquarters, Radnor, PA) and dosed as described above (**Dosing with 5-ALA**). Twenty-four hours after dosing, confocal images were acquired with Nikon A1R Confocal Microscope using 60X objective. Cells were excited at 405 nm and collected using 700/75 long pass filter. Fluorescence measurements from confocal images were analyzed using Fiji software [48]. Confocal imaging was performed quickly and with minimal white light exposure to avoid bleaching of PpIX fluorescence.

2.5. EV isolation

EVs were isolated from the conditioned media using ExoEasy kit [49] (ExoEasy Maxi Kit, Qiagen, Hilden, Germany). EVs were isolated from 20 ml of conditioned media. Briefly, media is allowed to reach room temperature and is mixed with a binding buffer in 1:1 ratio. The buffer-media is then loaded into affinity columns, washed and EVs are eluted using the ExoEasy EV elution buffer. EVs are then suspended in elution buffer and used for ISX analysis.

2.6. EGFR conditional transgenic mice

All mouse procedures were performed in accordance with Beth Israel Deaconess Medical Center's recommendations for the care and use of animals, and they were maintained and handled under protocols approved by the Institutional Animal Care and Use Committee. Cre/Lox-mediated conditional expression of the human EGF receptor vIII was achieved by stereotactic intracranial injections of an adenovirus expressing Cre recombinase (Gene Transfer Vector Core, University of Iowa, Iowa City, IA) as described in [50].

2.7. 5-ALA dosing in mice

Mice were monitored by weight, body conditioning, and behavioral symptoms for tumor burden. Pre-5-ALA blood samples were collected by submandibular puncture, blood was collected into a tube containing 3.8% Sodium Citrate. 20 mg/kg 5-ALA was injected intraperitoneally and mice were kept in the dark for three hours prior to post 5-ALA bleeds. Mice were deeply anesthetized with Ketamine/Xylazine (ketamine 125 mg/kg, xylazine 12.5 mg/kg) and blood was collected by cardiac puncture. Plasma was then separated from the hematocrit, aliquoted and stored at −80°C until ISX analysis. Demographics of the mice are reported in Table 1.

2.8. Ethics approval and consent to participate

All the participating patients signed the informed consent form, and the study was approved by the Internal Review Board (IRB) ethical committee of the Massachusetts General Hospital (2017P001581).

2.9. Patient characteristics

The study population ($n = 6$) consisted of patients 18 years or older with a newly identified T1-weighted gadolinium-enhancing lesion concerning for malignant glioma who underwent FGS using 5-ALA at the Massachusetts General Hospital. Pathology confirmed GBM diagnosis for all patients ($n = 6$). Samples from four patients were collected as part of a clinical trial (ClinicalTrials.gov Identifier: NCT02632370; 5-Aminolevulinic Acid (5-ALA) to Enhance Visualization of Malignant Tumor) to evaluate the safety and efficacy of Gliolan™ (Trademark name for 5-ALA in the trial) as a surgical adjunct to malignant glioma tumor resection. Two patients were given Gleolan (Trademark name for FDA approved ALA: ALA HCl, NX Development Corp., Lexington, KY) independent of the trial. Patients with contrast enhancing lesions were given an oral dose of 20 mg/kg 5-ALA, 3–5 h prior to FGS for glioma surgery as a part of standard of care. Patient demographics, MRI tumor volume, pathological diagnosis and the intensity of intraoperative fluorescence (as assessed by the operating neurosurgeon) is reported in Table 2. We characterized all avidly fluorescent tumors as '*avidly fluorescent*' and the tumors with either no fluorescence or background level of fluorescence as seen in normal cerebral cortex as '*minimally fluorescent*' (Fig. 7a). All protocols were approved by an institutional review board.

2.10. Patient plasma processing

Pre-5-ALA and the subsequent post 5-ALA plasma samples were collected prior to and ~3 h after 5-ALA administration. Whole blood samples were collected using K2 EDTA tubes with an inert gel barrier (BD Vacutainer® blood collection tubes) and centrifuged at 1100 x g for 10 min to separate the hematocrit from the plasma. Samples were then filtered using 0.8 μm filter and aliquoted into amber-colored cryovials (Polypropylene Microtubes, Analytical Sales and Services Inc., Flanders, NJ) to reduce any fluorescence bleaching caused by direct light exposure. All plasma samples were processed within 2 h of collection and stored at −80°C until ISX analysis. Precautions were taken to minimize the exposure to light during sample collection and processing. For 4 of the 6 patients, blood samples were collected 3–4 h after the oral administration of 5-ALA. While for patients P5 and P6, the post 5-ALA samples were collected 2 h and 5 h after 5-ALA dosing, respectively. For patient P3, pre-5-ALA blood draw were not obtained, hence we obtained 2-week postoperative plasma sample that we used as baseline.

Table 1
Mice demographics.

Mice	Age (days)	Sex	Diagnosis	Plasma collection post 5-ALA dosing (hours)	Tumor Fluorescence	Fold Change Post/Pre 5-ALA
Cl	100	M	Control	3	N/A	0.6
C2	100	M	Control	3	N/A	1
C3	100	M	Control	3	N/A	1.4
T1	76	M	Glioblastoma	3	Fluorescent	5.4
T2	87	M	Glioblastoma	3	Fluorescent	1.7

N/A = Not applicable.

2.11. ImageStream^x imaging flow cytometer

We used an ImageStream^x (ISX) MkII Imaging flow cytometer (IFC, Amnis Corporation, Seattle, WA, USA) equipped with two charged couple device (CCD) cameras and 12 spectral image detection channels (Ch 01- Ch 12): Ch 01 420–480 nm, Ch 02 480–560 nm, Ch 03 560–595 nm, Ch 04 595–660 nm, Ch 05 660–740 nm, Ch 06 740–800 nm, Ch 07 420–505 nm, Ch 08 505–570 nm, Ch 09 570–595 nm, Ch 10 595–660 nm, Ch 11 660–740 nm, Ch 12 740–800 nm; and 5 solid state excitation lasers: 405 nm laser, 488 nm laser, 561 nm laser, 592 nm laser, and 658 nm laser. Two channels (Ch 01 and Ch 09) were set to brightfield, permitting spatial coordination between cameras and Ch 06 was set to side scatter. INSPIRE version 200.1.620.0 instrument software was used for instrument setup, calibration and data acquisition. Upon each startup, the instrument calibration tool ASSIST® was performed to optimize performance and consistency. The advanced fluidic control of ISX, coupled with the presence of continuously running speed beads enable cell/particle enumeration using the "objects per ml" feature within the IDEAS® data analysis software. The samples were loaded and the events were collected as RIF files. 1,000 event single color compensation controls were collected (without BF or SSC) and later merged to create a compensation matrix for analysis. Once the RIF files were merged and compensated, a gating strategy was used for consistency. The ISX requires small volumes (25- 100 µL), in most cases we opted for 100 µL sample. Cells were centrifuged at 300 x g for 5 mins and resuspended in 100 µL of PBS for ISX analysis. For ISX analysis of EV samples, 30–100 µL conditioned media, ExoEasy isolated EVs, mice plasma and patient plasma was used. All samples were collected in eppendorf tubes covered with aluminum foil to minimize exposure to light. Detergent lysis of all samples was performed using 0.1% Triton^{TM} X-100 (Thermo Fisher Scientific, Waltham, MA) for 15 min at room temperature.

2.12. Optimization and calibration for EV analysis

ApogeeMix (Apogee Flow Systems, UK) and fluorescent-labeled liposomes (Avanti Lipids, USA) were used to optimize and calibrate ISX for EV analysis. ApogeeMix contained green beads 110 nm and 500 nm in size. Six preparations of liposomes were custom manufactured. Alexa Fluor 405, Alexa Fluor 555 and Alexa Fluor 647 liposomes, each of 100 and 200 nm sizes. The ApogeeMix were analyzed undiluted, while the liposomes were analyzed after 1 in 500 dilution in filtered PBS.

2.13. ISX analysis of cells

Cells were analyzed with fluidics set at low speed, sensitivity set to high, magnification at 40X and core size 10 µm. The 405 nm laser was set at 120 mW and side scatter SSC/785 nm laser at 1.00 mW. 100 µL samples were loaded and multiple 10,000 event files were acquired. RIF files were generated, merged, compensated and a gating strategy (Fig. 2) was used for consistency.

2.14. Gating strategy for cells

Gate R1(green): Aspect ratio and area of brightfield images (Ch 01) were used to gate for single cell events. Aspect ratio is the ratio of minor axis to major axis and is representative of shape and circularity of an event. Area is the measure of size. Single cells as detected by aspect ratio ~ 1.0 and uniform area. Gate R5 (red): Gradient RMS of brightfield images (Ch 01) was used to further analyze the R1 population to identify single cells in focus. Gradient RMS represents the sharpness quality of the image. Finally, R5 population was analyzed for fluorescence in Ch 11: λ 660–745 nm. The gated events were visually interrogated and verified (Fig. 2). Mean fluorescence intensity in Ch 11 in relative light units (RLU) was used for comparisons. For further details see [51,52].

2.15. EV analysis on ISX

Analysis was performed with fluidics set at low speed, sensitivity set to high, magnification at 60X, core size 7 µm, and the "Hide Beads" option unchecked prior to every acquisition in order to visualize speed beads in analyses. All parameters are stored in acquisition template except the latter, which requires unchecking prior to each acquisition. The lasers were run at maximal power to ensure maximal sensitivity: 405 nm (120 mW), 488 nm (200 mW), 561 nm (200 mW), and 642 nm (150 mW). To avoid the risk of coincident particle detection, EV samples were not run at concentrations greater than 1010 objects/ml [42]. The Flow Speed was stably maintained at around 44 and the Flow Speed Error CV was maintained under 0.2, and priming was done when the Flow Speed became unstable. Samples were allowed to run for 1–2 min prior to acquisition, to reach a stable Flow Speed and a low Flow Speed Error CV (Supplementary Fig. 3).

2.16. Collection strategy for EV analysis

R0 Collection Gate (white): Scatter plot of fluorescence intensity (Ch 11) vs. side scatter (Ch 06) was generated and R0 Collection Gate was Set to exclude the majority speed bead events. A minimum of 40,000 R0 Collection Gate events were collected. The runs were kept under 20 mins, even if 40,000 R0 events were not acquired (Supplementary Fig. 3).RIF files were generated, merged, compensated and a gating strategy (Fig. 3) was used for consistency.

2.17. Gating strategy for EVs

Alexa Fluor 647 100 nm-sized liposomes were nanoparticles used to optimize for EV gating strategy. Gate R1 (green): Population with a stable ISX Flow Speed was selected. Unstable portions of the run were excluded to minimize the bias caused by the variations in instruments fluidics as well so to remove artifactual events. Gate R2 (grey) was created to exclude doublets, triplets, debris and large aggregates. Aspect ratio and area of bright field images was used to gate out the population with large area and variable aspect ratio. Speed beads were included in the Gate R2

Table 2
Patient demographics.

Patient	Age	Sex	Diagnosis	Tumor Volume (cm^3)	Plasma collection post 5-ALA dosing (hours)	Intraoperative Fluorescence	Fold Change Post/Pre 5-ALA
PI	55	M	Glioblastoma	37.7	3	Avidly fluorescent	3.1
P2	72	F	Glioblastoma	28.8	3.5	Avidly fluorescent	2.3
P3	63	M	Glioblastoma	9.23	3	Avidly fluorescent	2.0
P4	73	M	Glioblastoma	2.53	3	Avidly fluorescent	1.6
P5	42	F	Glioblastoma	18.1	5	Minimally fluorescent	0.6
P6	51	M	Glioblastoma	21.2	2	Minimally fluorescent	0.9

N/A = Not applicable.

to have a reference population. Finally, Gate R3 (red) was created to encompass low side scattering events, that did not produce a brightfield image but demonstrated fluorescence in Ch 11: λ 660–745 nm. Inspire masking was used to detect fluorescent events in Ch 11 and spot counting feature was used to exclude swarming. The gated events were visually interrogated and verified. The positive events were expressed as objects/ml (Fig. 3). For further details see [36,41–43].

2.18. Nanoparticle tracking analysis (NTA)

Concentrations and particle sizes of EVs in conditioned media, ExoEasy isolated EVs, plasma of mice and humans were measured by NanoSight NTA (LM10, Malvern Inst. Ltd., UK). Samples were prepared in dilutions of 1:10 for media, 1:100 for EVs and 1:3000 for plasma of mice and humans. Dilutions were made with filtered PBS and measurements recorded in triplicates over 30 s, with manual monitoring of temperature and camera level set to 14. Analysis was performed using NTA v3.1 software, with detection threshold set to 7. All NTA EV concentration data was expressed in EVs / ml and EV size data in mode values.

2.19. Statistical analysis

Data are expressed as mean 95% confidence interval. Statistical analysis was performed using Microsoft Office Excel 2011 or Graph Pad Prism 8 software. The unpaired two-tailed Student's *t*-test was used for comparisons between groups. $^{*}p \leq 0.05$, $^{**}p \leq 0.01$, $^{***}p \leq 0.001$ was considered statistically significant. Comparisons were done between the samples of each patient before and after 5-ALA dosing. The same was done for the mice. Inter-patient or inter-mice comparisons were not performed due to heterogeneity in the pre-dosing background levels. The increase in the PpIX-positive EV counts was expressed as fold change due to heterogeneity in the background. The same unit of measurement was used for both pre and post-dosing patient/mice samples.

3. Results

3.1. Optimization of 5-ALA concentration in glioma cells for maximum viability and fluorescence intensity

Dosing of 5-ALA for cells in culture was established via *in vitro* testing of the human glioma Gli36 cell line. Glioma cells were seeded in a 6-well plate (250,000 cells/well) and dosed with increasing concentrations of 5-ALA (mock, 0.8 mM, 8 mM, 16 mM, 32 mM and 64 mM). Twenty-four hours after dosage of cells, we assessed mean fluorescence intensity in relative light units (RLU) using confocal microscopy (Fig. 1a and Supplementary Fig. 1a). We observed a decrease in fluorescence intensity with increasing concentrations of 5-ALA, and the maximum mean fluorescence intensity was observed with the 0.8 mM dose ($p = 0.0002$; Fig. 1b). The maximum cell viability was also noted with 0.8 mM (after the mock treated cells), and the viability showed an inverse dose-dependent correlation with increasing concentrations ($r^2 = 0.90$; Fig. 1c). Confocal microscopy also allowed us to visualize the increase in dead cells as 5-ALA dosage increased (Supplementary Fig. 1a). The decreasing fluorescence intensity with increasing concentrations of 5-ALA, is possibly a consequence of increasing cell death with the increasing concentration of the compound.

We next used ISX to determine the brightest possible PpIX cell fluorescence and the lowest rate of cell death to minimize the possibility of apoptotic particles released in the media. We used gating strategy to capture a homogeneous population of single cells with fluorescence in Ch 11 (λ660-745 nm; Fig. 2a–c). From this cell population, ISX analysis confirmed maximum mean fluorescence

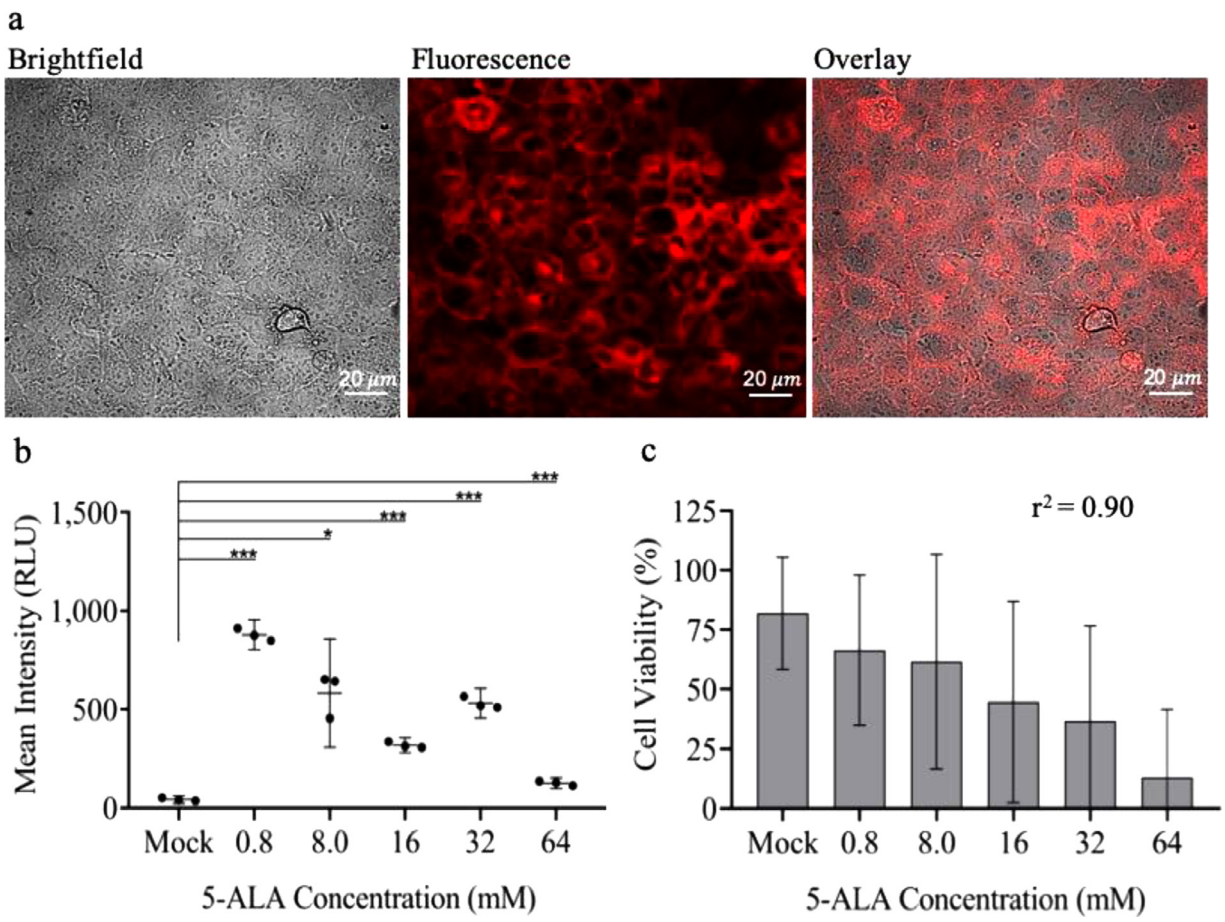

Fig. 1. Determining optimal 5-ALA dose for maximum fluorescence and viability of glioma cells (a) Confocal images of PpIX fluorescence in Gli36 cells treated with 0.8 mM 5-ALA dose for 24 h. Brightfield image (left), fluorescence image (center), overlay image (right). **(b)** Dot-plot showing PpIX fluorescence (mean intensity in relative light units, RLU) of Gli36 cells at different 5-ALA doses measured using confocal microscopy. **(c)** Histogram showing cell viability (%) of Gli36 cells at different 5-ALA doses measured using Countess II FL Automated Cell Counter. Data are mean 95% confidence interval ($n = 3$ biological replicates). $^{*}p \leq 0.05$, $^{**}p \leq 0.01$, $^{***}p \leq 0.001$, unpaired two-tailed Student's *t*-test.

intensity from cells dosed with the 0.8 mM concentration of 5-ALA (Fig. 2d) and a decreasing mean fluorescence intensity with increasing 5-ALA doses ($p = 0.001$; Supplementary Fig. 1b). After performing these experiments in three biological replicates, the 0.8 mM dose of 5-ALA consistently resulted in the highest fluorescence intensity and the lowest cell death rate (after mock). Findings were congruent between ISX and confocal microscopy, therefore we used the 0.8 mM concentration for all our subsequent *in vitro* experiments (Supplementary Fig. 1).

3.2. Optimization of ISX for EV analysis using nanoparticle-sized calibration beads and fluorophore-labeled liposomes

ISX is a high throughput and sensitive cytometer that allows interrogation of single fluorescence-positive nanoparticles with simultaneous visualization within brightfield, side scatter, and fluorescent channels. We used custom-made 100 and 200 nm sized Alexa Fluor 647 liposomes (excitation max λ650 nm, emission max λ665 nm) to optimize the gating strategy for single fluorescent EV detection. These liposomes represented nanoparticles of similar size and emission range of what would be expected with PpIX-labeled EVs, and therefore served as a positive control. Liposomes were excited with a 658 nm laser (100 mW) and analyzed. We first selected the region of the run where the fluids were stable (Fig. 3a) and then gated out large aggregates with high area and low aspect ratio (Fig. 3b). Finally, we gated in our population of interest as low side-scattering fluorescent events in Ch 11 which were not captured in brightfield (Fig. 3c). Simultaneously, we analyzed all other channels and found no overlapping events with those observed in Ch 11, confirming the specificity of our Alexa Fluor 647 liposomes to Ch 11.

We based our fluorescence thresholds by first analyzing PBS buffer, our negative control (Fig. 3d, Supplementary Fig. 2). ISX was able to detect 100 and 200 nm fluorescent liposomes, both separately and in combination, yet we were unable to clearly differentiate between 100 nm and 200 nm subpopulations, likely due to the similarity in size and limits in sensitivity of the instrument (Fig. 3d, Supplementary Fig. 2). On the contrary, we were able to clearly visualize the subpopulations of the ApogeeMix calibration beads mix of 110 nm and 500 nm (Supplementary Fig. 2a). In order to confirm the specificity of nanoparticle detection of different fluorescence spectra, we also analyzed 100 nm and 200 nm-sized Alexa Fluor 405 and Alexa Fluor 555 liposomes (Supplementary Fig. 2b,c). Finally, we confirmed that we were unable to detect fluorescent events following detergent lysis of liposomes, which supports the notion that the fluorescent events that we had previously detected were indeed true liposomes (Fig. 3b, Supplementary Fig. 2b,c). For all ISX runs of nanoparticles, we used the instrument settings as previously reported in the literature (Supplementary Fig. 3) [36,42].

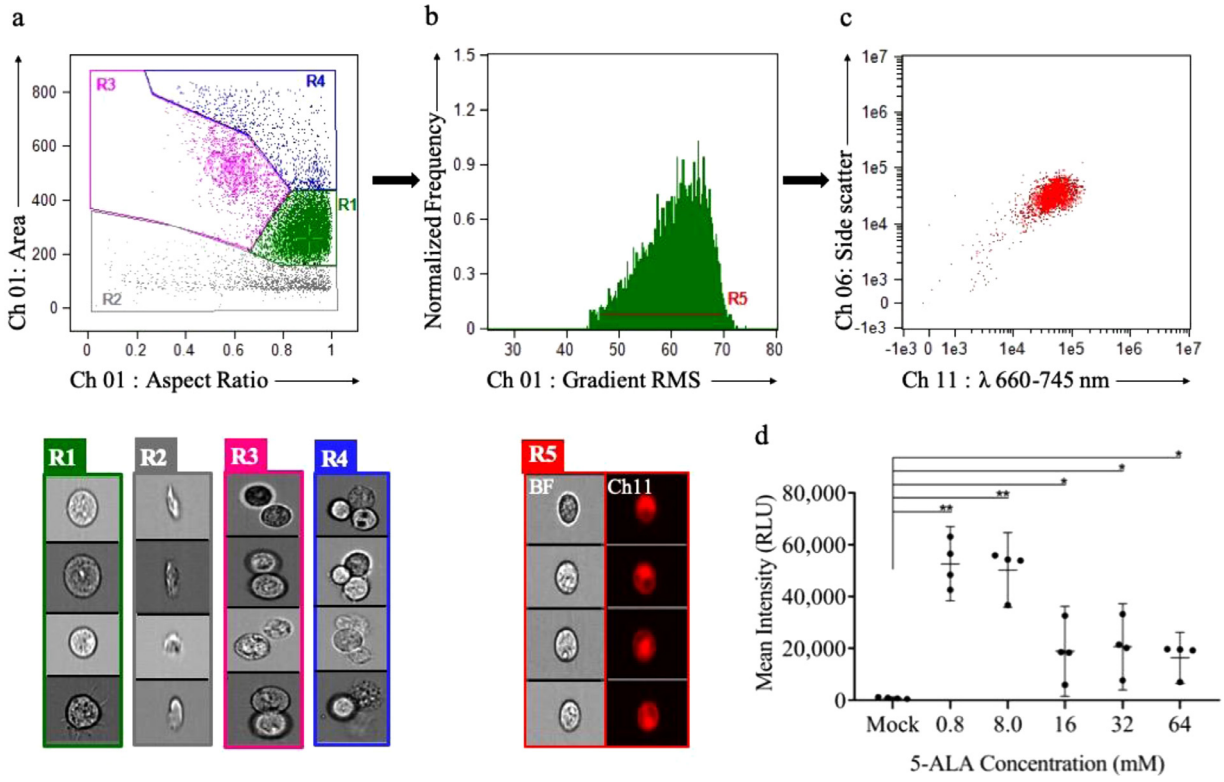

Fig. 2. ISX analysis for glioma cells dosed with 5-ALA. Visual interrogation and gate setting to demonstrate PpIX fluorescence: **(a)** ISX scatter plot of Gli36 cells by aspect ratio (x-axis, shape and measure of circularity) vs. area (y-axis, size). Gate R1 (green): Single cells as detected by aspect ratio ~1.0 and uniform area. Gate R2 (gray): Cell debris as detected by varying aspect ratio and low area. Gate R3 (pink): Doublet cells as detected by an aspect ratio ~0.5 and high area. Gate R4(blue): Triplet cells as detected by an aspect ratio ~1.0 and high area. Ch 01 brightfield images of cells (R1, green), cell debris (R2, gray), doublet cells (R3, pink), triplet cells (R4, blue). **(b)** The representative histogram of gradient RMS (Ch 01) vs. normalized frequency to identify cells in focus based on the sharpness of the image. Gate R5 (red): Gating of single cells in focus with PpIX fluorescence (Ch 11: λ 660–745 nm). R5-gated brightfield images (Ch 01) and corresponding fluorescence images (Ch 11) demonstrating PpIX fluorescence. **(c)** Scatter plot of fluorescence intensity (Ch 11) vs. side scatter (Ch 06) showing a homogeneous clustered population of focused, single cells demonstrating PpIX fluorescence (Ch11). **(d)** Dot-plot showing PpIX fluorescence (mean intensity in relative light units, RLU) of Gli36 cells at different 5-ALA doses showing maximal mean intensity at 0.8 mM. Data are mean 95% confidence interval ($n = 4$ biological replicates). $^{*}p \leq 0.05$, $^{**}p \leq 0.01$, $^{***}p \leq 0.001$, unpaired two-tailed Student's *t*-test. (For interpretation of the references to colour in this figure legend, the reader is referred to the web version of this article.)

3.3. Glioma cells, but not HBMVEC, dosed with 5-ALA release PPIX-positive EVs that can be detected using ISX

Next, we determined the specificity of PpIX-positive EVs released from 5-ALA dosed cancer cells (Gli36) cells as compared to non-cancer cells (HBMVEC). We first analyzed negative controls of PBS buffer alone, PBS buffer mixed with 5-ALA, as well as Elution Buffer from a commercial EV-isolation kit in order to establish background fluorescent signal (Fig. 4a). Next, we dosed both the glioma cells and HBMVEC with 0.8 mM of 5-ALA and PBS as control. Conditioned media was collected 24 h later, centrifuged at low speed (300 x g for 10 min) to remove debris, and filtered through a 0.8 μm filter to remove large particles. We then analyzed the purified media on ISX using our previously established gating strategy (see above). We found a 247-fold increase of PpIX-positive EVs in glioma cells dosed with 5-ALA compared to mock dosing (Fig. 4b), while HBMVEC dosed with 5-ALA yielded a 6-fold increase in PpIX-positive EVs compared to mock dosing (Fig. 4c). These findings suggest that the increased PpIX accumulation known to occur preferentially in glioma cells lead to a significantly higher release of PpIX-containing EVs, a phenomenon not as pronounced in healthy cells. To confirm that the fluorescent events were indeed extracellular vesicles, we performed a lysis step and found a significantly reduced signal (Supplementary Fig. 4a,b).

To further validate that we were indeed working with EVs we used a commercial kit to isolate EVs from 5-ALA dosed cells [49]. Twenty ml of media was used as input into the ExoEasy kit, which can isolate intact EVs by membrane affinity [49], and eluted them in 400 μl of elution buffer. We then analyzed the EVs on ISX and found a 20-fold increase of PpIX-positive EVs released from glioma cells dosed with 5-ALA compared to mock dosing (Fig. 4d), while HBMVEC dosed with 5-ALA showed a 7-fold increase in PpIX-positive EVs compared to mock dosing (Fig. 4e). We again performed a lysis step and found a significantly reduced signal (Supplementary Fig. 4c,d).

3.4. Exposure to white light leads to bleaching of PPIX-positive EVs and loss of fluorescent ISX signal

We then investigated why there was a lower yield of PpIX-positive EVs isolated using the kit as compared to direct analysis of the conditioned media. Bleaching of PpIX fluorescence from white light exposure has been well established for tumor tissue analysis [53]. With this in mind, our main hypothesis was that the decrease in signal was due to the increase in white light exposure that occurred with kit processing. To test this hypothesis, we exposed EVs from glioma cells dosed with 5-ALA to white light for 20 min prior to ISX analysis. We observed an 8-fold decrease in PpIX-positive EVs as compared to EVs isolated without prolonged exposure to white light (Fig. 5). Given the significant effect of white light on the loss of ISX signal intensity from PpIX-positive EVs, for our *in vivo* studies we chose to analyze EVs directly from unprocessed plasma.

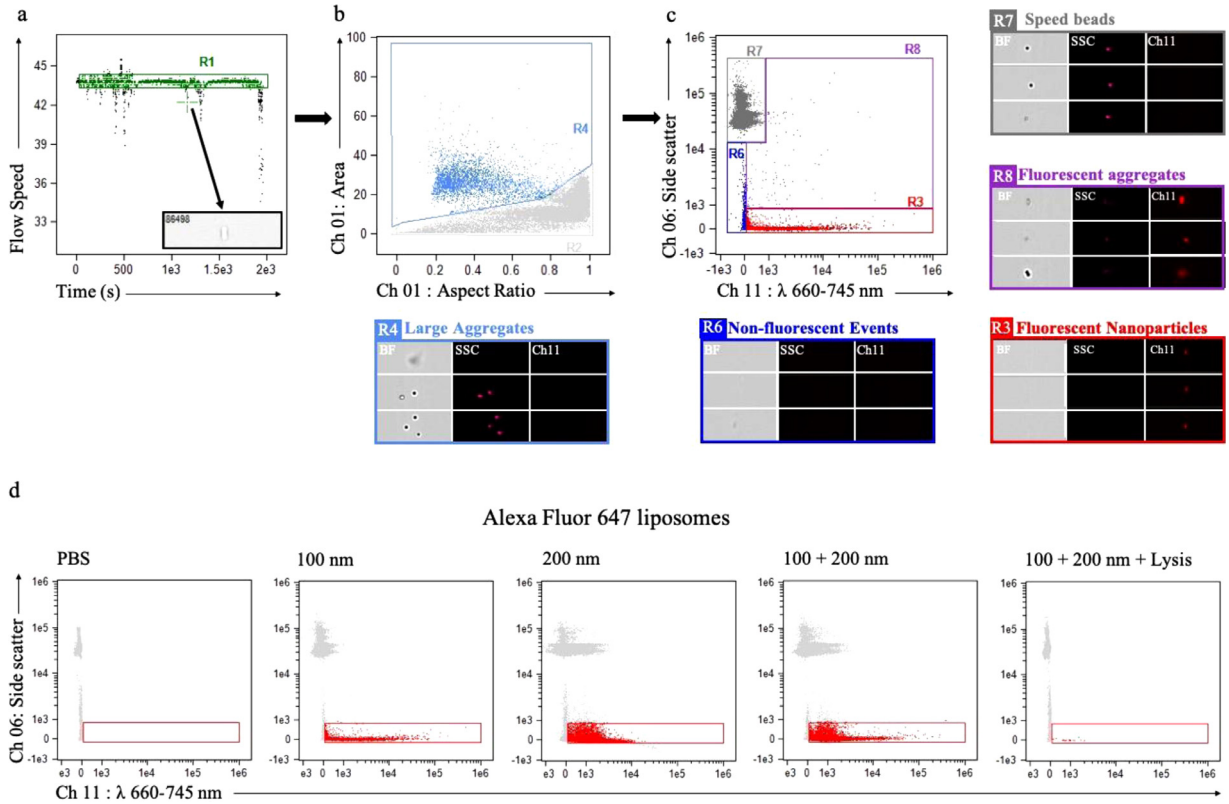

Fig. 3. ISX analysis and characterization of nanoparticles using 100 nm Alexa Fluor 647 (650/665) liposomes. **(a)** ISX scatter plot of time vs. flow speed; Gate R1 (green): selection of a population where the ISX flow speed is stable, excluding artifactual events from unstable flow speed (gray box) **(b)** ISX scatter-plot of aspect ratio vs. area of brightfield images (Ch 01); Gate R2 (gray): gated population for fluorescent liposome analysis, excluding doublets, triplets, debris and large aggregates (Gate R4, light blue). Representative images of R4 events visualized on brightfield (Ch 01, BF), side scatter (Ch06, SSC), and fluorescence spectrum (Ch 11). **(c)** ISX scatter plot of fluorescence intensity (Ch 11) vs. side scatter (Ch 06) with R3 gate (red) representing 100 nm sized Alexa Fluor 647 liposomes with low side scatter and fluorescence in Ch 11 and are not captured on brightfield images. Gate R6 (royal blue) represents non-fluorescent events, which are not captured on brightfield images and have low side scatter. Gate R7 (gray) represents speed beads, which are captured on brightfield images, have high side scatter, and are non-fluorescent. Gate R8 (purple) represents fluorescent aggregates, captured on brightfield images, and have high side scatter. **(d)** ISX scatter plot of fluorescence intensity (Ch 11) vs. side scatter (Ch 06) with PBS buffer (control, left), and Alexa Fluor 647 liposomes of sizes 100 nm, 200 nm, and in combination. The fluorescent events were not detected after detergent lysis. (For interpretation of the references to colour in this figure legend, the reader is referred to the web version of this article.)

3.5. PpIX-positive EVs can be detected in plasma of glioma-bearing mice dosed with 5-ALA but not in control mice

We next sought to explore the specificity of PpIX-positive EV signal from the plasma of glioma-bearing mice as compared to control mice after dosage with 5-ALA (Table 1, Fig. 6a). We first sampled baseline plasma (pre-5-ALA) from 3 control mice and 2 glioma mice. Three hours following weight-based 5-ALA dosing, the plasma of all mice was sampled again (post-5-ALA). The mice were kept in the dark following drug dosage, as were all plasma samples. Given the findings of diminished PpIX signal with *in vitro* use of EV-isolation kit, we decided to analyze pure plasma. ISX analysis demonstrated a significant increase ($p = 0.004$) in PpIX-positive EVs in the glioma-bearing mice following 5-ALA administration as compared to pre-5-ALA levels while we did not observe a similar increase in the control mice (Fig. 6b–d, Supplementary Fig. 5). The brains of the tumor-bearing mice were obtained immediately following the terminal plasma collection and were confirmed to contain avidly fluorescent tumor under blue light-filtered microscope. These findings suggest that, despite systemic uptake of 5-ALA, a rise in PpIX EVs occur only when a glioma is present, and therefore, the EVs are specific to the glioma itself. As determined by NTA, the size and concentrations of EVs from the mice was similar between pre- and post-5-ALA dosing (Supplementary Fig. 7a,b).

3.6. Patients with avidly fluorescent malignant gliomas observed during FGS release PPIX-positive EVs into circulating plasma

We interrogated the plasma of 6 patients who underwent FGS to determine the PpIX-positive EV signal before and after dosage with 5-ALA. All patients enrolled in this study underwent surgical management at our institution. We observed tumors with avid fluorescence in 4 of 6 patients, whereas the remaining 2 patients had minimal fluorescence, all under blue light microscopy (Fig. 7a,b, Table 2).

ISX analysis of pure plasma in patients with avidly fluorescent tumors demonstrated a highly significant increase ($p = 0.00009$) in PpIX-positive EVs in the post-5-ALA samples as compared to pre-5-ALA samples. We did not observe a similar rise from the intraoperative samples obtained from the patients whose tumors had minimal fluorescence (Fig. 7c). We also established that a 1.0-fold change or greater increase of post-5-ALA EVs over baseline levels represented a true positive signal (Fig. 7d). Furthermore, this fold change in signal significantly and positively correlated with each patient's enhancing tumor volume ($r^2 = 0.888$, Fig. 7e).

We were also able to track Patient 2 longitudinally and observed a 2.3-fold increase in PpIX-positive EVs in post-5-ALA plasma compared to pre-5-ALA levels, followed by a sustained return to baseline levels at 2 weeks and 6 weeks post-operatively

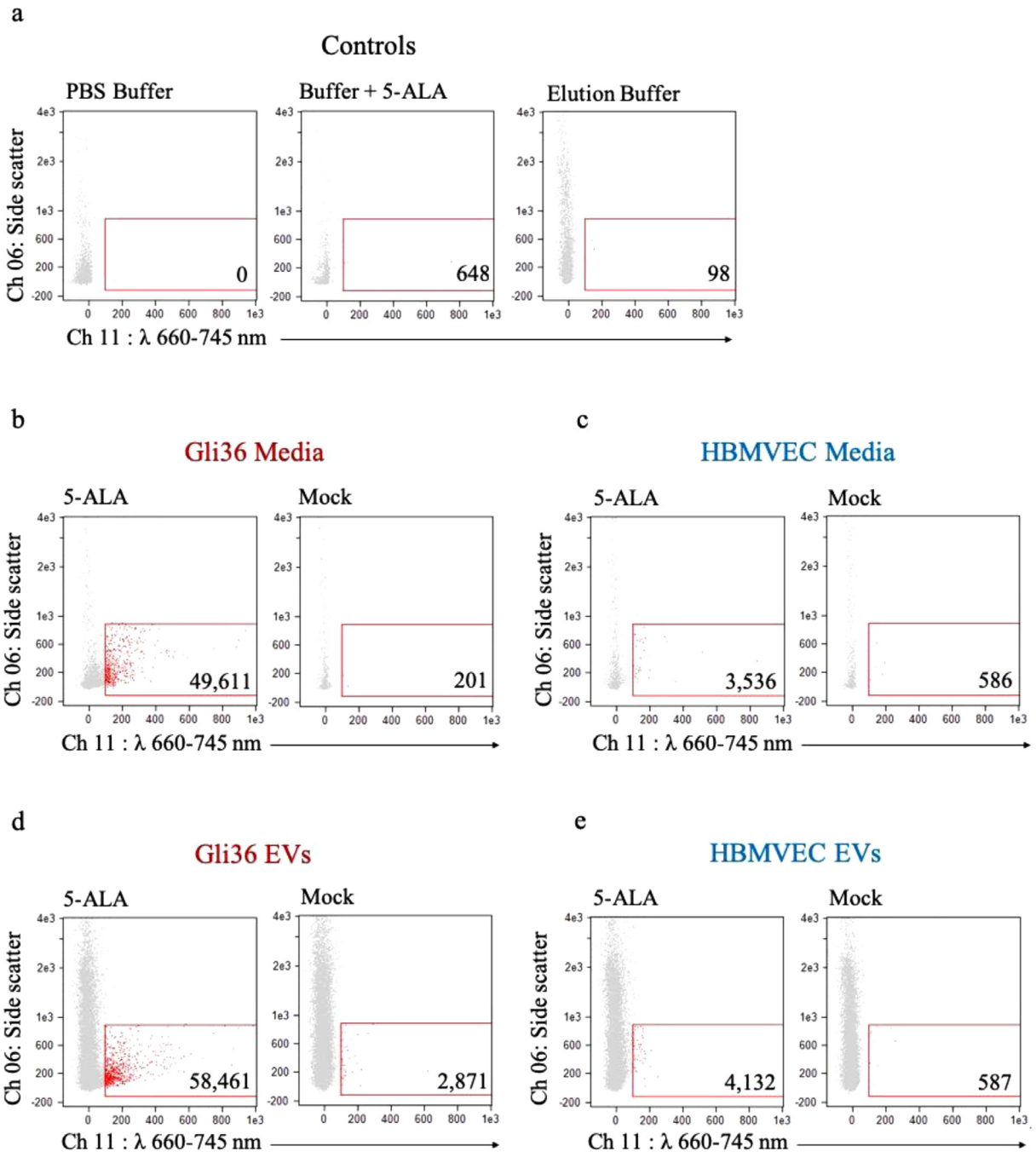

Fig. 4. ISX characterization of conditioned media and EVs derived from 5-ALA dosed Gli36 cells and HBMVEC. (a) Control samples: ISX scatter plots of PBS buffer only (left), buffer with 5-ALA (center), and elution buffer following processing with ExoEasy Kit (right). **(b)** ISX scatter plot of media from 5-ALA dosed (left) and mock dosed (right) Gli36 cells. **(c)** ISX scatter plot of media from 5-ALA dosed (left) and mock dosed (right) HBMVEC. **(d)** ISX scatter plot of EVs isolated from 5-ALA dosed (left) and mock dosed (right) Gli36 cells. **(e)** ISX scatter plot of EVs isolated from 5-ALA dosed (left) and mock dosed (right) HBMVEC.

(Fig. 7f). The lack of avid fluorescence in 2 of our patient tumors was thought to be due to poor timing, as the tumor resection and plasma collection for these patients occurred at the shortest and longest intervals following 5-ALA administration. The fluorescence observed by the operating neurosurgeon in these 2 patients was consistent with either no fluorescence or a background fluorescence seen in normal cerebral cortex, which is very minimal compared to the usual avid fluorescence seen in the other 4 patients. As determined by NTA, the size and concentrations of EVs from the mice was similar between pre- and post-5-ALA dosing (Supplementary Fig. 7c,d).

4. Discussion

This study demonstrates that malignant gliomas with avid intraoperative PpIX fluorescence release PpIX-positive EVs that can be detected in circulating plasma using IFC. The ability to perform a minimally-invasive liquid biopsy for patients with malignant glioma, either through plasma or other biofluids, would greatly expand our ability to diagnose and track treatment response for this challenging and lethal disease. EVs serve as important cellular surrogates, carrying information in the form of proteins, RNA, and DNA, and are in greater abundance in circulating fluid compared

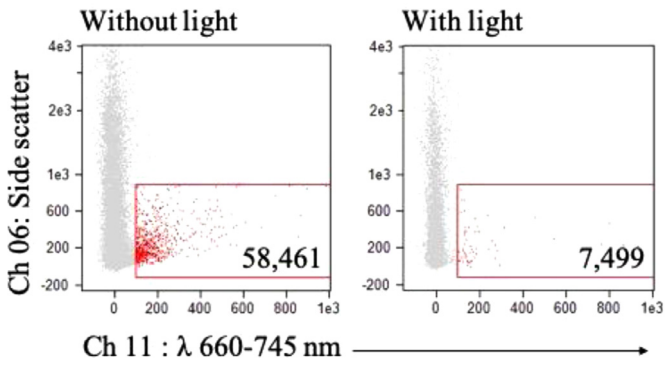

Fig. 5. ISX characterization of Gli36 EVs following white light exposure. ISX scatter plot of EVs from conditioned media of Gli36 cells dosed with 5-ALA for 24 h, isolated using a commercial kit, before (left) and after (right) 20 min of exposure to white light.

to other circulating markers like circulating tumor cells (CTCs) or cell-free DNA (cfDNA) [54]. This has led to significant recent interest in the clinical applications of EVs as biomarkers for many cancers [55–58]. However, the isolation of sEVs and differentiation of EV subpopulations (eg., differentiation of normal vs tumor EVs in the plasma) remains one of the major challenges within the field [32,59,60,61]. Using state-of-the-art IFC, we detected and quantified tumor-derived PpIX-positive sEVs released from 5-ALA dosed glioma cells *in vitro*, glioma bearing xenograft models dosed with 5-ALA, and malignant glioma patients undergoing 5-ALA based FGS.

Given that most conventional flow cytometers were designed to measure cells or biologic particles in the 2–30 μm range, it has not been until recently that cytometers have been optimized to detect particles below 500 nm in size [37,41,42,46]. In this report, we have optimized ISX to detect and quantify individual fluorescent EVs, allowing us to test a novel liquid biopsy strategy in brain tumor patients. Prior to interrogating patient plasma, we first established a PpIX-positive EV signal specific to the glioma-bearing mouse plasma, with plasma from control mice remaining at background levels, both pre- and post-5-ALA dosing ($p = 0.004$). The preferential release of PpIX-containing EVs from glioma cells *in vitro* and in our pre-clinical *in vivo* rodent model set the stage for our efforts to clinically detect these PpIX-positive EVs in brain tumor patients undergoing FGS with 5-ALA as a proof-of-principle. In 6 patients analyzed, we demonstrated that patients with avidly fluorescent tumors (4/6; 66%) indeed contained circulating PpIX-positive EVs at levels significantly higher than their pre-dosing background ($p = 0.00009$), and this rise in signal correlated highly with enhancing tumor volumes ($r^2 = 0.888$). For 2 patients with minimally fluorescent tumors, the PpIX-positive EV signal remained at or below their baseline background levels (Fig. 7a–c, Supplementary Fig. 6). Our study is therefore consistent with previous reports that show circulating PpIX levels only rise after the administration of 5-ALA when tumors are present [62,63]. Although background levels remained consistently low among both of our pa-

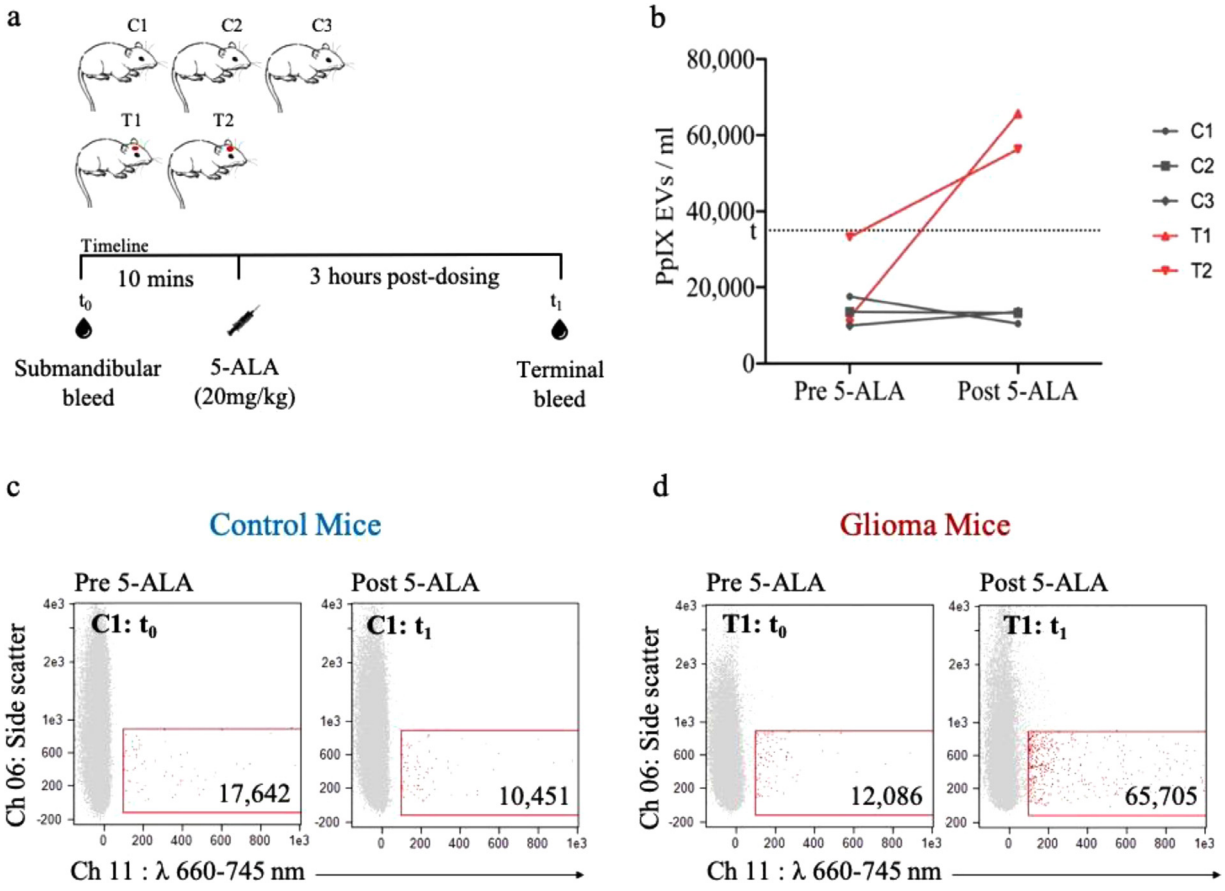

Fig. 6. ISX characterization of plasma-derived PpIX-positive EVs from control and glioma-bearing mice dosed with 5-ALA. (a) Overview of the experiment **(b)** Line plot showing pre-5-ALA and post-5-ALA PpIX-positive EV levels for the control (gray) and glioma (red) mice. The dotted line represents the threshold (t) of background fluorescent signal prior to 5-ALA dosing based on this population. **(c)** ISX scatter plot of representative control mouse plasma before 5-ALA (left) and 3 h post- 5-ALA (right). **(d)** ISX scatter plot of representative glioma-bearing mouse plasma before 5-ALA (left) and 3 h post-5-ALA (right). (For interpretation of the references to colour in this figure legend, the reader is referred to the web version of this article.)

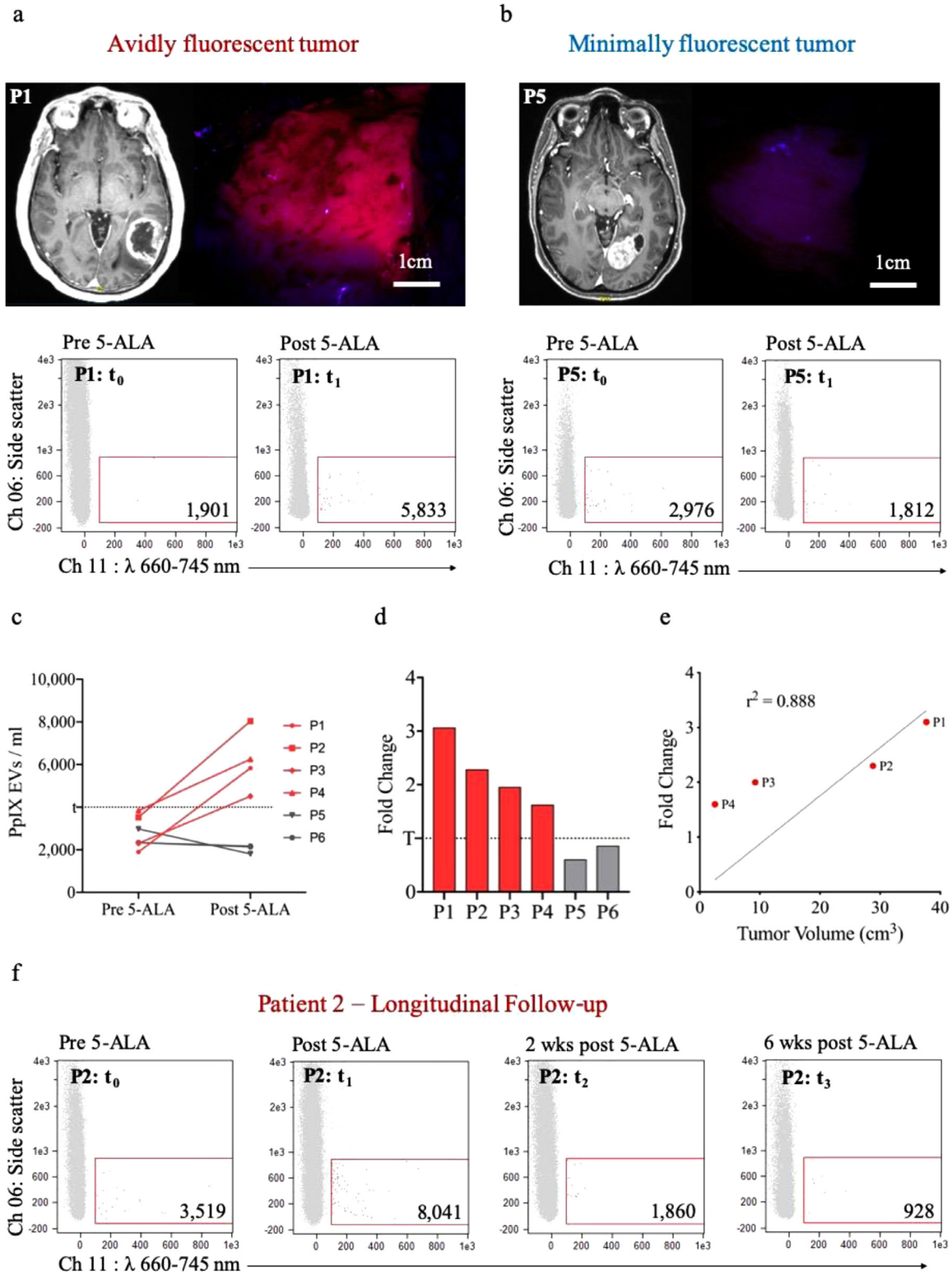

Fig. 7. ISX characterization of plasma-derived PpIX-positive EVs from patients with malignant glioma following 5-ALA administration for FGS with both avidly fluorescent and minimally fluorescent tumors. (a) Avidly fluorescent tumor: The T1-post-gadolinium-contrast axial MRI (left) shows the posterior left temporal tumor which demonstrated avid intraoperative fluorescence under the blue light of the microscope (right); ISX scatter plot of representative patient plasma before 5-ALA (left) and following 5-ALA (right). (b) Minimally fluorescent tumor: The T1-post-gadolinium-contrast axial MRI shows the left occipital tumor (left) which demonstrated minimal intraoperative fluorescence under the blue light of the microscope (right); ISX scatter plot of representative patient plasma before 5-ALA (left) and following 5-ALA (right). (c) Line-plot of pre-5-ALA and post-5-ALA levels for patients with avidly fluorescent tumors (red) and minimally fluorescent tumors (gray). The dotted line represents the threshold (t) of background fluorescent signal prior to 5-ALA dosing based on this population. (d) Bar graph indicating the fold change (post-5-ALA/pre-5-ALA levels) of PpIX-positive EV signal for patients with avidly fluorescent tumors (red) and patients with minimally fluorescent tumors (gray). (e) Pearson correlation of enhancing tumor volumes and fold change of PpIX-fluorescent EV signal from the 4 patients with avidly fluorescenct tumors (f) ISX scatter plots of Patient 2 plasma: pre-5-ALA, post-5-ALA (intraoperative, 3.5 h post-dosing), 2 weeks post-FGS, and 6 weeks post-FGS; wks = weeks. (For interpretation of the references to colour in this figure legend, the reader is referred to the web version of this article.)

tient groups, there was some inter-patient variability which limited our ability to establish a confident background cutoff valid across all individuals. Because of this heterogeneity in background signal, a fold change of >1.0 (PpIX-positive EVs post/pre-5-ALA levels) is what we determined the cutoff for a true positive tumor signal (Fig. 7d). Interestingly, we also determined that for patients with this true positive signal, the tumor volumes significantly correlated with the resulting fold change, which strongly supports the notion that these PpIX-positive EVs are truly glioma-derived. In one case (Patient 2), PpIX-positive EV levels increased 2.3-fold with fluorescent-guided tumor resection and this signal returned to background levels in the following weeks (Fig. 7f), suggesting that the rise in PpIX-positive EVs represented a true tumor signal and not a random phenomenon. This work is an important proof-of-concept of plasma-based EV detection technology for potential clinical applications in both diagnosis and monitoring of malignant glioma. In addition, this could be combined with other tools to sort and isolate tumor EV subpopulations, which would allow for further characterization of the genetic cargo within tumor EVs.

While most patients with malignant gliomas have fluorescent tumors [64,65], 2 of our cases lacked avid intraoperative fluorescence and, in turn, did not demonstrate a rise in PpIX-positive EV signal. This was an important observation because it demonstrated the critical importance of the timing of plasma sampling following administration of 5-ALA in order to optimize the potential of detecting PpIX EVs. Studies indicate that, when administered correctly, intraoperative fluorescence has greater than 90% sensitivity and specificity for detecting newly diagnosed and recurrent malignant gliomas [64,65]. Tumors lacking fluorescence, a false negative, usually occur when resection is undertaken too quickly following 5-ALA ingestion or in cases of high tumor necrosis [53]. Our two cases likely fell within both of these categories, with Patient 6 plasma sampling and tumor resection occurring 2 h following dosing, which was likely too early. We also had a lack of tumor fluorescence for Patient 5, which was carried out at 5 h after dosing, the longest interval between dosing and surgery in our group. Furthermore, the tumor was highly necrotic, which could be contributing factor for the lack of fluorescence observed intraoperatively. This suggests that the optimal time window for plasma sampling for PpIX-positive EV signal occurs at 3–4 h post-5-ALA administration.

The limitation of our study is the small sample size of patients, as a larger cohort of patients would allow for robust quantification of PpIX positive EVs following 5-ALA administration. With collection of plasma from larger cohort of patients, strict standardization of sample collection, handling and avoidance of light exposure are essential. In addition, analysis of plasma from healthy controls following 5-ALA administration would allow better determination of background fluorescent EVs.

Overall, this work adds to a small but growing body of literature that uses IFC to explore circulating EVs as markers of glioma diagnosis and prognosis. Ricklefs et al. used IFC to analyze sEVs and distinct subpopulation of EVs both in *in vitro* and *in vivo* models of malignant glioma [41]. They first showed that EVs from cell lines could be tagged with fluorescent-labeled antibodies to EV-specific tetraspanins CD9, CD63 and CD81 and found that glioblastoma cell lines secrete EVs with significantly elevated proportions of CD81+ and CD63+ tetraspanins compared to normal cells. They also found similar results looking at the serum of human glioblastoma patients, with total numbers of double positive CD63+/CD81+ and CD9+/CD63+ EVs increased compared to healthy controls. Glabo et al. used IFC to measure serum-based exosomes positive for survivin following an anti-survivin vaccine in patients with malignant glioma [43]. They showed that not only could they find survivin tumor markers on CD9+ exosomes from patient serum, but, by IFC measurements, lower levels of these exosomes following vaccination were associated with longer progression-free survival. Because EVs are also involved in intercellular communication and immune response, this recent work has highlighted changes in circulating EV levels that are believed to reflect presence of and changes in tumor but not directly from the tumor itself. Our study characterizes plasma-derived EVs that are of glioma origin and, considering the high correlation with the tumor presence (and volume), this suggests a PpIX-positive EV signal can offer a powerful "window" into the primary tumor's presence and status.

The detection of PpIX-positive EVs in patients with malignant glioma paves the way for clinical validation studies of this technology as a strategy for non-invasive brain tumor diagnosis and monitoring. In addition, further developments in EV sorting technology will offer the opportunity for combining this technique for protein and nucleic acid characterization.

Funding sources

This work is supported by grants U01 CA230697 (BSC, LB), UH3 TR000931 (BSC), P01 CA069246 (BSC, AC), K12CA090354 (PSJ), U19 CA179563 (AC).

The funding sources had no role in the study design, interpretation of results, writing the manuscript or decision to submit the manuscript for the publication. The authors have not been paid to write this article by any entity. The corresponding author has full access to all the data and assumes final responsibility for the decision to submit for publication.

Author contributions

L.B., B.S.C., F.H.H., conceptualized the study; L.B., B.S.C., supervised the study and designed the experiments; A.Y., P.S.J., and E.L., performed microscopy and ImageStream experiments. J.S. and C.A., enrolled patients in clinical trial and collected human specimen. A.Y., P.S.J., B.D., and A.C., performed the mice experiment. A.Y., J.T., and I.G., performed control experiments using beads and liposomes using flow cytometry. S.M., reviewed ImageStream workflow. A.Y., P.S.J., L.B., and B.S.C., analyzed all data, generated figures and wrote the paper with input from all authors.

Declaration of Competing Interest

B.S. Carter, L. Balaj, P.S. Jones and A. Yekula are co-inventors on a pending patent for the use of 5-ALA in the diagnosis of malignant gliomas. The other authors declare no competing interests.

Acknowledgments

This publication is part of the NIH Extracellular RNA Communication Consortium paper package and was supported by the NIH Common Fund's exRNA Communication Program.

Imaging was performed in the Microscopy Core of the Program in Membrane Biology, which is partially supported by a Centre for the Study of Inflammatory Bowel Disease Grant DK043351 and a Boston Area Diabetes and Endocrinology Research Center (BADERC) Award DK057521. The Nikon A1R confocal system is supported by NIH shared instrumentation grant 1S10 RR031563-01. The Amnis ImageStream MkII located in the Department of Pathology Flow, Image and Mass Cytometry Core was purchased using an NIH Shared Instrumentation Grant 1S10OD012027-01A1 Amnis ISX (FIP).

Supplementary materials

Supplementary material associated with this article can be found, in the online version, at doi:10.1016/j.ebiom.2019.09.025.

References

[1] Wen PY, Kesari S. Malignant gliomas in adults. N Engl J Med 2008;359:492–507.
[2] Vuorinen V, Hinkka S, Färkkilä M, Jääskeläinen J. Debulking or biopsy of malignant glioma in elderly people - a randomised study. Acta Neurochir (Wien) 2003;145:5–10.
[3] Stummer W, et al. Fluorescence-guided surgery with 5-aminolevulinic acid for resection of malignant glioma: a randomised controlled multicentre phase III trial. Lancet Oncol 2006;7:392–401.
[4] Stepp H, Stummer W. 5-ALA in the management of malignant glioma. Lasers Surg Med 2018;50:399–419.
[5] Zimmermann M, Stan AC. PepT2 transporter protein expression in human neoplastic glial cells and mediation of fluorescently tagged dipeptide derivative β-Ala-Lys-Nε-7-amino-4-methyl-coumarin-3-acetic acid accumulation. J Neurosurg 2010;112:1005–14.
[6] Hagiya Y, et al. Expression levels of PEPT1 and ABCG2 play key roles in 5-aminolevulinic acid (ALA)-induced tumor-specific protoporphyrin IX (PpIX) accumulation in bladder cancer. Photodiagnosis Photodyn Ther 2013;10:288–95.
[7] Ennis SR, et al. Transport of 5-aminolevulinic acid between blood and brain. Brain Res 2003;959:226–34.
[8] Navone NM, Polo CF, Frisardi AL, Andrade NE, del C Baille AM. Heme biosynthesis in human breast cancer—mimetic '*in vitro*' studies and some heme enzymic activity levels. Int J Biochem 1990;22:1407–11.
[9] Hinnen P, et al. Biochemical basis of 5-aminolaevulinic acid-induced protoporphyrin IX accumulation: a study in patients with (pre)malignant lesions of the oesophagus. Br J Cancer 1998;78:679–82.
[10] Schwartz DI, et al. Differentiation-dependent photodynamic therapy regulated by porphobilinogen deaminase in B16 melanoma. Br J Cancer 2004;90:1833–41.
[11] Greenbaum L, Gozlan Y, Schwartz D, Katcoff DJ, Malik Z. Nuclear distribution of porphobilinogen deaminase (PBGD) in glioma cells: a regulatory role in cancer transformation. Br J Cancer 2002;86:1006–11.
[12] Teng L, et al. Silencing of ferrochelatase enhances 5-aminolevulinic acid-based fluorescence and photodynamic therapy efficacy. Br J Cancer 2011;104:798–807.
[13] Ohgari Y, et al. Mechanisms involved in δ-aminolevulinic acid (ALA)-induced photosensitivity of tumor cells: relation of ferrochelatase and uptake of ALA to the accumulation of protoporphyrin. Biochem Pharmacol 2005;71:42–9.
[14] Krieg RC, Fickweiler S, Wolfbeis OS, Knuechel R. Cell-type specific protoporphyrin IX metabolism in human bladder cancer *in vitro*. Photochem Photobiol 2000;72:226–33.
[15] Kobuchi H, et al. Mitochondrial localization of ABC transporter ABCG2 and its function in 5-Aminolevulinic acid-mediated protoporphyrin IX accumulation. PLoS ONE 2012;7:e50082.
[16] Peng Q, et al. Distribution of 5-aminolevulinic acid-induced porphyrins in noduloulcerative basal cell carcinoma. Photochem Photobiol 1995;62:906–13.
[17] Leunig A, Betz CS, Heinrich P, Janda P, Baumgartner R. [Fluorescence staining of oral and laryngeal cancer after application of 5-aminolevulinic acid]. Laryngorhinootologie 2002;81:807–14.
[18] Vansevičiūtė R, Venius J, Letautienė S. 5-Aminolevulinic acid-based fluorescence diagnostics of cervical preinvasive changes. Medicina (B Aires) 2014;50:137–43.
[19] Murayama Y, et al. Staging fluorescence laparoscopy for gastric cancer by using 5-aminolevulinic acid. Anticancer Res 2012;32:5421–7.
[20] Shishkova N, Kuznetsova O, Berezov T. Photodynamic therapy for gynecological diseases and breast cancer. Cancer Biol Med 2012;9:9–17.
[21] Millon SR, et al. Preferential accumulation of 5-aminolevulinic acid-induced protoporphyrin IX in breast cancer: a comprehensive study on six breast cell lines with varying phenotypes. J Biomed Opt 2010;15:018002.
[22] Hadjipanayis CG, Widhalm G, Stummer W. What is the surgical benefit of utilizing 5-Aminolevulinic acid for fluorescence-guided surgery of malignant gliomas? Neurosurgery 2015;77:663–73.
[23] Santiago-Dieppa DR, et al. Extracellular vesicles as a platform for 'liquid biopsy' in glioblastoma patients. Expert Rev Mol Diagn 2014;14:819–25.
[24] Muller L, et al. Exosomes isolated from plasma of glioma patients enrolled in a vaccination trial reflect antitumor immune activity and might predict survival. Oncoimmunology 2015;4:e1008347.
[25] Shi R, et al. Exosomal levels of miRNA-21 from cerebrospinal fluids associated with poor prognosis and tumor recurrence of glioma patients. Oncotarget 2015;6:26971–81.
[26] Evans SM, et al. Initial evidence that blood-borne microvesicles are biomarkers for recurrence and survival in newly diagnosed glioblastoma patients. J Neurooncol 2016;127:391–400.
[27] Koch CJ, et al. Microvesicles as a biomarker for tumor progression versus treatment effect in radiation/temozolomide-treated glioblastoma patients. Transl Oncol 2014;7:752–8.
[28] Gourlay J, et al. The emergent role of exosomes in glioma. J Clin Neurosci 2017;35:13–23.
[29] Vrij Jde, et al. Glioblastoma-derived extracellular vesicles modify the phenotype of monocytic cells. Int J Cancer 2015;137:1630–42.
[30] Ricklefs F, et al. Extracellular vesicles from high-grade glioma exchange diverse pro-oncogenic signals that maintain intratumoral heterogeneity. Cancer Res 2016;76:2876–81.
[31] van Niel G, D'Angelo G, Raposo G. Shedding light on the cell biology of extracellular vesicles. Nature Rev Mol Cell Biol 2018;19:213–28.
[32] Willms E, et al. Cells release subpopulations of exosomes with distinct molecular and biological properties. Sci Rep 2016;6.
[33] Yáñez-Mó M, et al. Biological properties of extracellular vesicles and their physiological functions. J Extracell Vesicles 2015;4:27066.
[34] Roy S, et al. Navigating the landscape of tumor extracellular vesicle heterogeneity. Int J Mol Sci 2019;20.
[35] Welsh JA, Holloway JA, Wilkinson JS, Englyst NA. Extracellular vesicle flow cytometry analysis and standardization. Front Cell Dev Biol 2017;5:78.
[36] Mastoridis S, et al. Multiparametric analysis of circulating exosomes and other small extracellular vesicles by advanced imaging flow cytometry. Front Immunol 2018;9:1583.
[37] Lannigan J, Nolan JP, Zucker R. Measurement of extracellular vesicles and other submicron size particles by flow cytometry. Cytometry A 2016;89:109–10.
[38] Pospichalova V, et al. Simplified protocol for flow cytometry analysis of fluorescently labeled exosomes and microvesicles using dedicated flow cytometer. J Extracell Vesicles 2015;4:25530.
[39] Nolan JP, Duggan E. Analysis of individual extracellular vesicles by flow cytometry. Method Molecul Biol 2017:79–92.
[40] Camacho V, Toxavidis V, Tigges JC. Characterization of extracellular vesicles by flow cytometry. Method Molecul Biol 2017:175–90.
[41] Ricklefs FL, et al. Imaging flow cytometry facilitates multiparametric characterization of extracellular vesicles in malignant brain tumours. J Extracell Vesicles 2019;8:1588555.
[42] Lannigan J, Erdbruegger U. Imaging flow cytometry for the characterization of extracellular vesicles. Methods 2017;112:55–67.
[43] Galbo PM Jr, et al. Circulating CD9+/GFAP+/survivin+ exosomes in malignant glioma patients following survivin vaccination. Oncotarget 2017;8:114722–35.
[44] Headland SE, Jones HR, D'Sa ASV, Perretti M, Norling LV. Cutting-edge analysis of extracellular microparticles using imagestreamx imaging flow cytometry. Sci Rep 2015;4.
[45] Erdbrügger U, et al. Imaging flow cytometry elucidates limitations of microparticle analysis by conventional flow cytometry. Cytometry A 2014;85:756–70.
[46] Görgens A, et al. Optimisation of imaging flow cytometry for the analysis of single extracellular vesicles by using fluorescence-tagged vesicles as biological reference material. J Extracell Vesicles 2019;8:1587567.
[47] Patel AP, et al. Single-cell RNA-seq highlights intratumoral heterogeneity in primary glioblastoma. Science 2014;344:1396–401.
[48] Schindelin J, et al. Fiji: an open-source platform for biological-image analysis. Nat Methods 2012;9:676–82.
[49] Enderle D, et al. Characterization of RNA from exosomes and other extracellular vesicles isolated by a novel spin column-based method. PLoS ONE 2015;10:e0136133.
[50] Zhu H, et al. Oncogenic EGFR signaling cooperates with loss of tumor suppressor gene functions in gliomagenesis. Proc Natl Acad Sci USA 2009;106:2712–16.
[51] Samsel L, et al. Imaging flow cytometry for morphologic and phenotypic characterization of rare circulating endothelial cells. Cytometry B Clin Cytom 2013;84:379–89.
[52] Basiji DA, Ortyn WE, Liang L, Venkatachalam V, Morrissey P. Cellular image analysis and imaging by flow cytometry. Clin Lab Med 2007;27:653–70.
[53] Stummer W, et al. Intraoperative detection of malignant gliomas by 5-aminolevulinic acid-induced porphyrin fluorescence. Neurosurgery 1998;42:518–25 discussion 525–6.
[54] Bettegowda C, et al. Detection of circulating tumor DNA in early- and late-stage human malignancies. Sci Transl Med 2014;6 224ra24.
[55] Vader P, Breakefield XO, Wood MJA. Extracellular vesicles: emerging targets for cancer therapy. Trends Mol Med 2014;20:385–93.
[56] Roy S, Hochberg FH, Jones PS. Extracellular vesicles: the growth as diagnostics and therapeutics; a survey. J Extracell Vesicles 2018;7:1438720.
[57] Rennert RC, Hochberg FH, Carter BS. ExRNA in biofluids as biomarkers for brain tumors. Cell Mol Neurobiol 2016;36:353–60.
[58] Hallal S, et al. The emerging clinical potential of circulating extracellular vesicles for non-invasive glioma diagnosis and disease monitoring. Brain Tumor Pathol 2019. doi:10.1007/s10014-019-00335-0.
[59] Giebel B. On the function and heterogeneity of extracellular vesicles. Ann Transl Med 2017;5 150–150.
[60] Gould SJ, Raposo G. As we wait: coping with an imperfect nomenclature for extracellular vesicles. J Extracell Vesicles 2013;2.
[61] Rupert DLM, Claudio V, Lässer C, Bally M. Methods for the physical characterization and quantification of extracellular vesicles in biological samples. Biochim Biophys Acta Gen Subj 2017;1861:3164–79.
[62] Inoue K, et al. Porphyrins as urinary biomarkers for bladder cancer after 5-aminolevulinic acid (ALA) administration: the potential of photodynamic screening for tumors. Photodiagn Photodyn Ther 2013;10:484–9.
[63] Ishizuka M, et al. Porphyrins in urine after administration of 5-aminolevulinic acid as a potential tumor marker. Photodiagn Photodyn Ther 2011;8:328–31.
[64] Stummer W, Stepp H, Wiestler OD, Pichlmeier U. Randomized, prospective double-blinded study comparing 3 different doses of 5-Aminolevulinic acid for fluorescence-guided resections of malignant gliomas. Neurosurgery 2017;81:230–9.
[65] Stummer W, et al. *In vitro* and *in vivo* porphyrin accumulation by C6 glioma cells after exposure to 5-aminolevulinic acid. J Photochem Photobiol B 1998;45:160–9.